Available online at www.sciencedirect.com
SCIENCE DIRECT®
ELSEVIER
Journal of Magnetism and Magnetic Materials 293 (2005) 151–161
Journal of magnetism and magnetic materials
www.elsevier.com/locate/jmmm

Microstructural investigation of ternary alloyed magnetic nanoparticles

Daniela Sudfeld[a,*], Inga Ennen[a], Andreas Hütten[a], Ute Golla-Schindler[b], Heiner Jaksch[c], Günter Reiss[a], Daniel Meißner[d], Klaus Wojczykowski[d], Peter Jutzi[d], Wahib Saikaly[e], Gareth Thomas[e]

[a]*Thin Films and Nanostructures, Department of Physics, University of Bielefeld, Universitätsstr. 25, D-33615 Bielefeld, Germany*
[b]*Institute of Mineralogy, University of Münster, Corrensstr. 24, 48149 Münster, Germany*
[c]*Carl Zeiss NTS GmbH, Carl-Zeiss-Str. 56, 73447 Oberkochen, Germany*
[d]*Inorganic Chemistry III, Department of Chemistry, University of Bielefeld, Universitätsstr. 25, D-33615 Bielefeld, Germany*
[e]*CP2M, Case 221, Faculty of Sciences and Technology of Saint-Jérôme, 13397 Marseille cedex 20, France*

Available online 18 April 2005

Abstract

Analytical transmission electron microscopy is a proper method so as to uncover microstructure and composition of novel magnetic nanocrystals potentially used as biological markers. The focus of this study is the preparation and characterization of the $(Fe_{1-x}Co_x)_{1-y}Pt_y$ alloyed nanoparticles utilizing high-resolution transmission electron microscopy and dispersive X-ray analyses.

PACS: 87.64.Ee; 81.07.Bc; 81.16.Be; 81.16.Dn

Keywords: Transmission electron microscopy; Nanoparticles; Energy dispersive X-ray analysis; FeCo; FePt; FeCoPt; Magnetic alloys; Synthesis

1. Introduction

Novel ligand stabilized magnetic nanocrystals which could be interesting for the next generation as markers for biological applications have been synthesized by various chemical preparation routes.

The potential of some of these nanocrystals has been evaluated answering the question whether colloidal synthesized superparamagnetic or ferromagnetic Co, FePt, CoFePt and FeCo nanocrystals with superior magnetic moments [1–7] could replace the iron oxide particles as magnetic carriers

*Corresponding author. Tel.: +49 521 106 5420; fax: +49 521 106 6046.
E-mail address: dsudfeld@physik.uni-bielefeld.de (D. Sudfeld).

0304-8853/$ - see front matter © 2005 Published by Elsevier B.V.
doi:10.1016/j.jmmm.2005.01.055

in in vitro separation and therapeutic in vivo technology. Therefore, the magnetophoretic mobility μ_m in the same liquid medium has been compared and the magnetic analysis has revealed that $Fe_{50}Co_{50}$ nanoparticles are superior from the magnetophoretic mobility point of view [1,2]. Finally, one goal of magnetic drug targeting should be that a maximum concentration of drug should be easily administered and transported to the site of choice with the least amount of magnetic particles [8]. One step to reach this request could be the use of $Fe_{50}Co_{50}$ nanoparticles, because calculations [1,2] have shown that there is only a $\frac{1}{25}$ or $\frac{1}{21}$ of the number of nanoparticles typed $Fe_{50}Co_{50}$ necessary which are deposited on a bead compared to the number of Fe_3O_4 or Fe_2O_3 particles per bead to gain the same efficiency.

The particles have been subsequently studied utilizing high-resolution transmission electron microscopy (HRTEM) aiming for the particles lattice structure. One advantage of this characterization technique is the possibility to simultaneously analyze the phase structure as well as the composition of nanocrystals. Using energy dispersive X-ray spectroscopy (EDX) in nanoprobe mode and electron energy-loss spectroscopy (EELS) the composition of individual Co, FePt, CoFePt and FeCo alloyed nanoparticles could be determined.

In addition, the nanoparticles have been investigated by using a field emission scanning electron microscope (FESEM) equipped with a special scanning transmission electron microscope (STEM) unit. STEM is a combination of the transmission and scanning electron microscopy and allows a less-time consuming imaging of electron transparent specimens in SEM microscopes with a better resolution.

The objective of our research is the development of magnetic nanoparticles which are surrounded by different steric organic ligands enabling the link to biotechnological applications. The size-controlled preparation and characterization of $(Fe_{1-x}Co_x)_{1-y}Pt_y$ alloyed nanoparticles comparing HRTEM and the more quantitative dispersive X-ray (XRD) analyses so as to reveal their microstructure are discussed in detail.

2. Materials and chemical preparation

Co [1–3], FePt [6,7], FeCo [1,2] and CoFePt alloyed nanocrystals have been synthesized with different nanocrystalline size distributions and concentration ratios. Hence, FeCoPt nanocrystals have been fabricated in mainly different ways as is given in the reaction scheme in Fig. 1. Firstly, preparation method PM1, following the chemical preparation route recently proposed by Chen et al. [9] the ternary alloyed particles have been produced with cobalt acetylacetonate. Secondly, the cobalt acetylacetonate has been substituted by dicobaltoctacarbonyl, $Co_2(CO)_8$. In detail, the synthesis to prepare FePt nanoparticles found by Sun et al. has been varied inasmuch that $Co_2(CO)_8$ had been injected into the solution in the presence of platinum acetylacetonate, $Pt(acac)_2$, and iron-pentacarbonyl, $Fe(CO)_5$. The cobalt carbonyl has been injected at the same temperature (ca. 100 °C) as the $Fe(CO)_5$ to allow a two-step-preparation process, preparation method PM2. To produce bigger particles, preparation method PM3, which are found to be more than double the size of the FeCoPt particles described above the $Co_2(CO)_8$ has been added in an o-dichlorobenzene refluxing bath (181 °C) according to the preparation route by the work of Puntes [3]. At last, preparation method PM4, FeCoPt have been prepared in another different way in which Pt particles have been synthesized separately and in the next step heated to reflux again and during this process

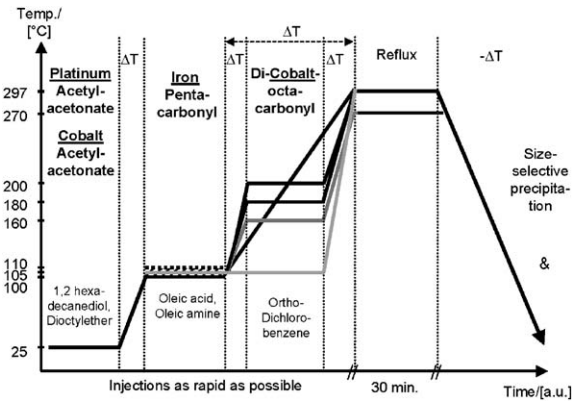

Fig. 1. Scheme of the reaction to produce FeCoPt nanoparticles by high-temperature solution-phase synthesis.

$Fe(CO)_5$ and $Co_2(CO)_8$ have been injected into the solution at 120 or 180 °C, respectively.

All steps in the preparation methods have been carried out under standard airless conditions.

3. Experimental methods

To obtain specimens for microstructural and magnetic characterization, about 2 μl of the solutions were dropped onto carbon coated transmission electron microscopy (TEM) Cu grids or onto glass or silicon oxide substrates. Conventional transmission electron microscopy (TEM) studies were performed using a Philips CM 100. High-resolution characterization (HRTEM) including EDX was carried out with a Philips CM 200 Super TWIN. As reported in Refs. [1–2,10] the EDX-spectra of FeCo alloyed nanoparticles were taken in the nanoprobe mode with a spot size of 12 nm allowing to average the composition of only a few nanoparticles. The field emission scanning electron microscope (FESEM) used is a Gemini Supra 55 VP from LEO Elektronenmikroskopie GmbH

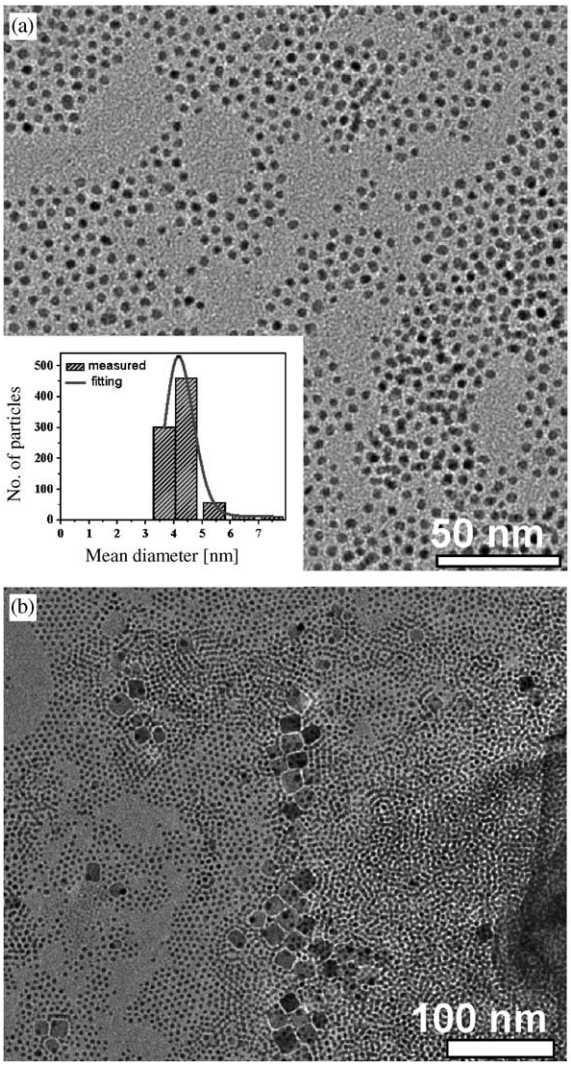

Fig. 2. Bright-field image made by TEM of FePt nanoparticles of different shapes. The nanospheres (a) have a size of 4–5 nm taken from the mean particle size distribution (inset). The nanocubes (b) have an edge length of approximately 18 nm.

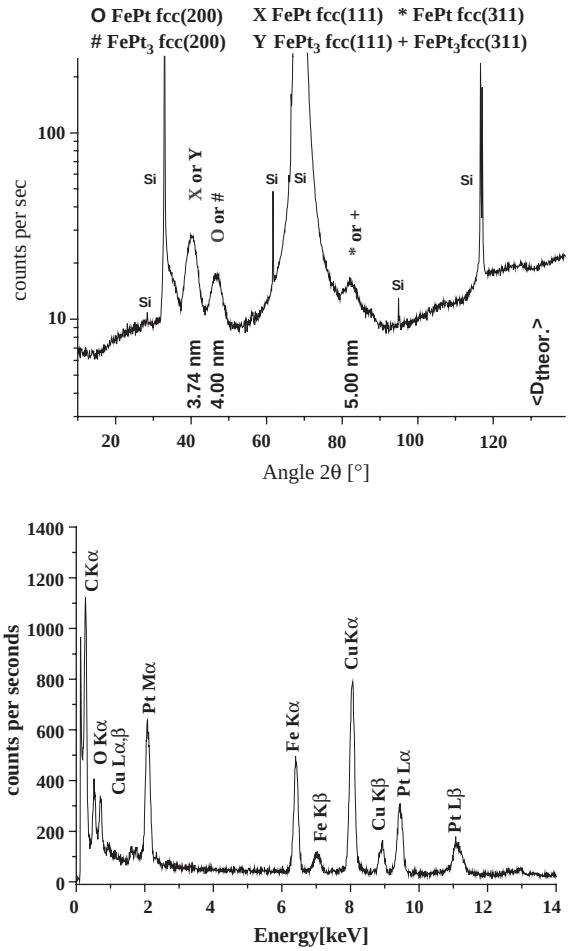

Fig. 3. EDX (a) quantified by TEM and XRD (b) measurements of FePt nanoparticles.

(now Zeiss NTS GmbH) with a multi mode Scanning Transmission Electron detection system (STEM), which is highly sensitive on the different information coming from bright field, dark field or orientation dark field. These different signals are separated and detected directly and can be combined individually to enhance or visualize the different data.

Additional TEM observations were carried out on an ultra high resolution JEOL 2010F with a field emission gun operating at 200 kV and equipped with a Gatan imaging filter (GIF), which allows for electron energy-loss spectroscopy (EELS) and chemical mapping. To investigate

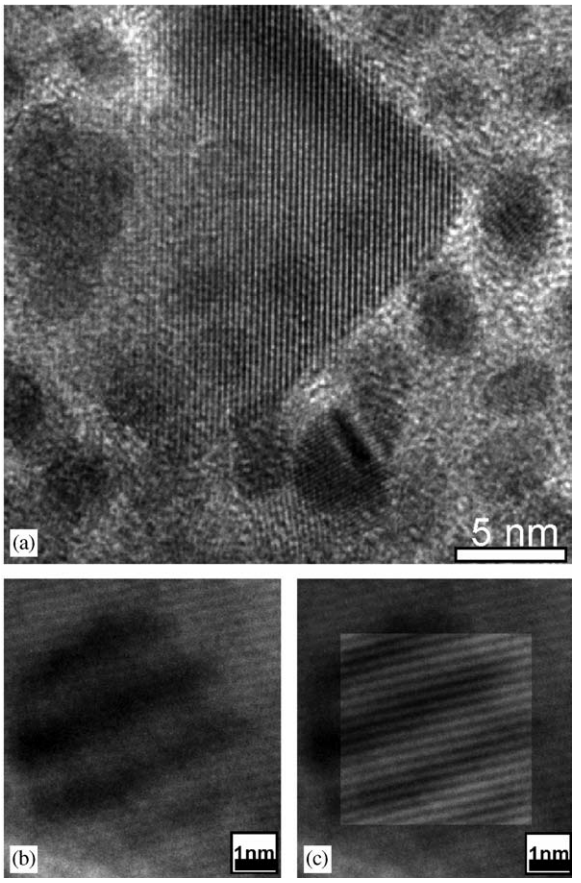

Fig. 4. Bright-field TEM images of FePt particles of different shapes (a,b) with the FFT filtered image (c) taken from the spheres. The measured lattice spacings of the FePt nanocube (square length = 18.83 nm) and the 5 nm sized FePt nanosphere indicate a $FePt_3$ FCC (1 0 0) orientation. The rotation moiré originates from the superposition of two different lattice-plane spacings which are rotated by a small angle to each other. The lattice-plane spacings have to be found Fe FCC (1 1 0), FePt FCC (1 1 1) or $FePt_3$ FCC (2 0 0) orientation.

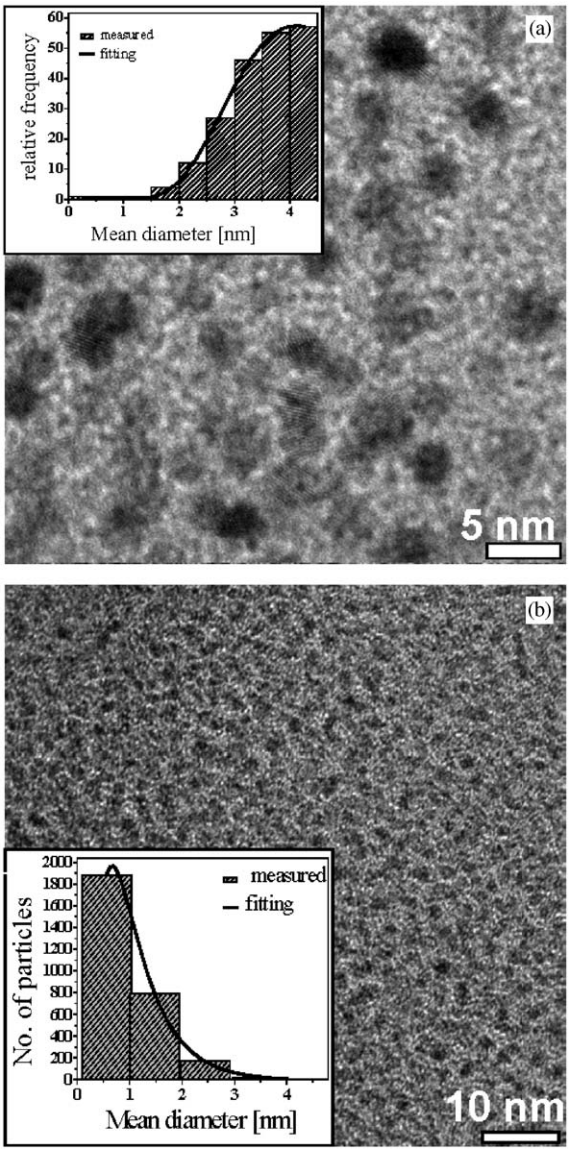

Fig. 5. Bright-field images of $Fe_4Co_2Pt_1$ nanoparticles are given with their corresponding size distributions. EDX by HRTEM analysis reveals a composition of $Fe_{2.8}Co_{1.0}Pt_{4.4} \pm 5\%$ for the particles prepared by PM2 (b). From the LogNormal size distribution a mean particle diameter $\langle D \rangle = 0.95 \pm 0.59$ nm has been determined. The mean particle diameter of $Fe_{1.8}Co_{1.0}Pt_{5.5} \pm 5\%$ particles prepared by PM3 is $\langle D \rangle = 4.63 \pm 0.34$ nm (a).

the formation of CoO and FeO at the particle surfaces of the FePt and FeCo alloyed particles EELS was used to analyze the components of the particles. The method is based on the energy-loss of fast electrons interacting with material when they traversed a thin specimen in a TEM. The edges observed in the EELS spectra are ionization energies and are labelled according to the ionized subshell [11,12].

In addition, for large particles microstructural characterization was carried out employing X-ray diffraction (XRD) using a Philips X'Pert Pro MPD with Cu K_α radiations with a wavelength of $\lambda = 0.154056$ nm. The theoretical particle

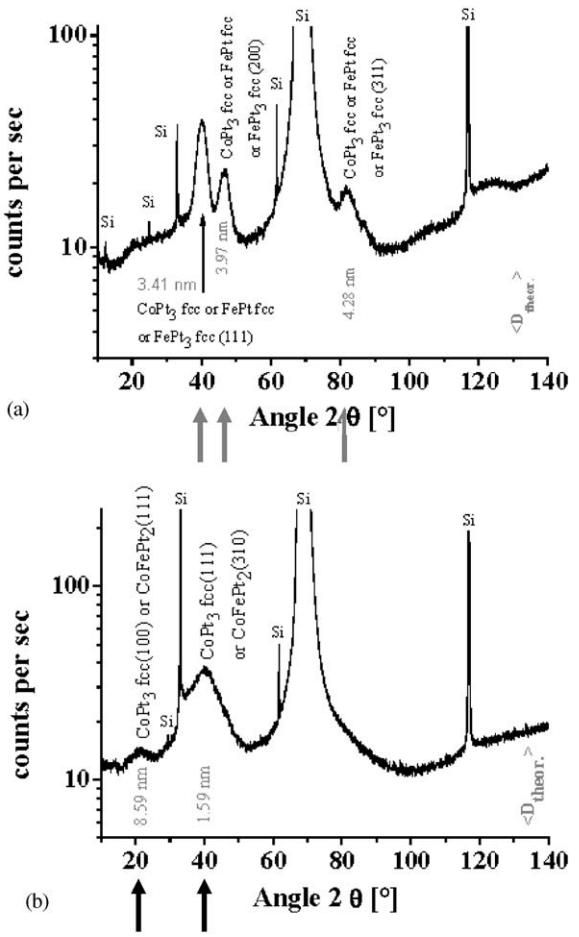

Fig. 6. The sample of $Fe_{1.8}Co_{1.0}Pt_{5.5} \pm 5\%$ (PM3) deposited on a silicon oxide substrate show XRD-peaks (marked in (a)) belonging to either $CoPt_3$ FCC phase or FePt FCC or $FePt_3$ FCC. XRD analyses (b) show that FeCoPt nanoparticles have been crystallized in inter alia in $CoFePt_2$ phase which explains the untypically peak positions at smaller angles 45°. The theoretical particle diameters D_{theor} could each be estimated from the full-width at half-maximum (FWHM) of the corresponding diffraction peaks by the formula from Scherrer.

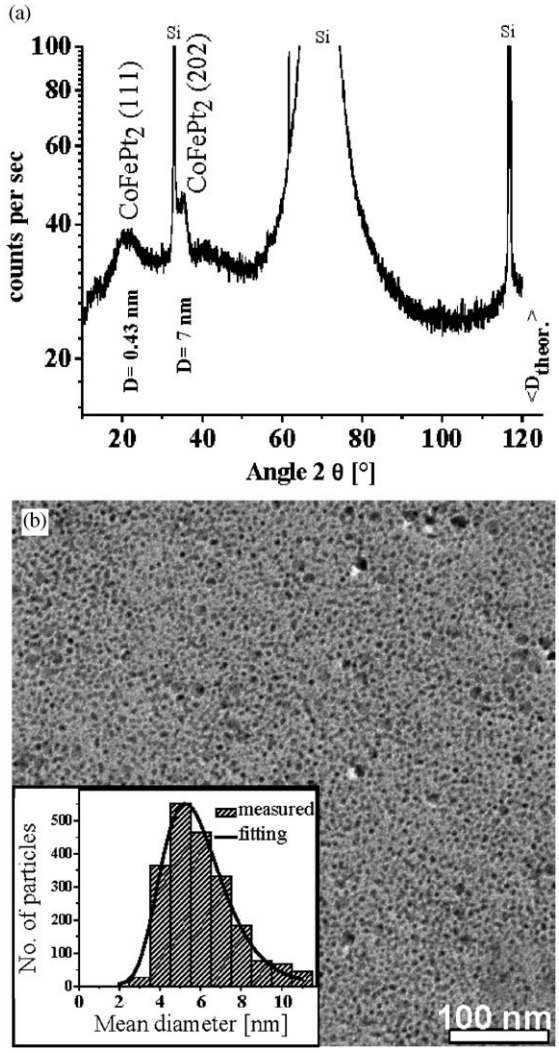

Fig. 7. XRD analyses in (a) clearly show that these FeCoPt nanoparticles prepared by PM4 are crystallized into the $CoFePt_2$ phase with the peak positions of circa 20° belonging to the (1 1 1) orientation and circa 35° to (2 0 2) orientation. The mean particle diameter quantified by the TEM bright-field image given in Fig. 7b is $\langle D \rangle = 5.66 \pm 0.76$ nm (b).

diamters D_{theor} which are calculated from the data of the corresponding peaks are also given in the presented XRD spectra. Each could be estimated from the full-width at half-maximum (FWHM) of the corresponding diffraction peaks by the formula from Scherrer [13].

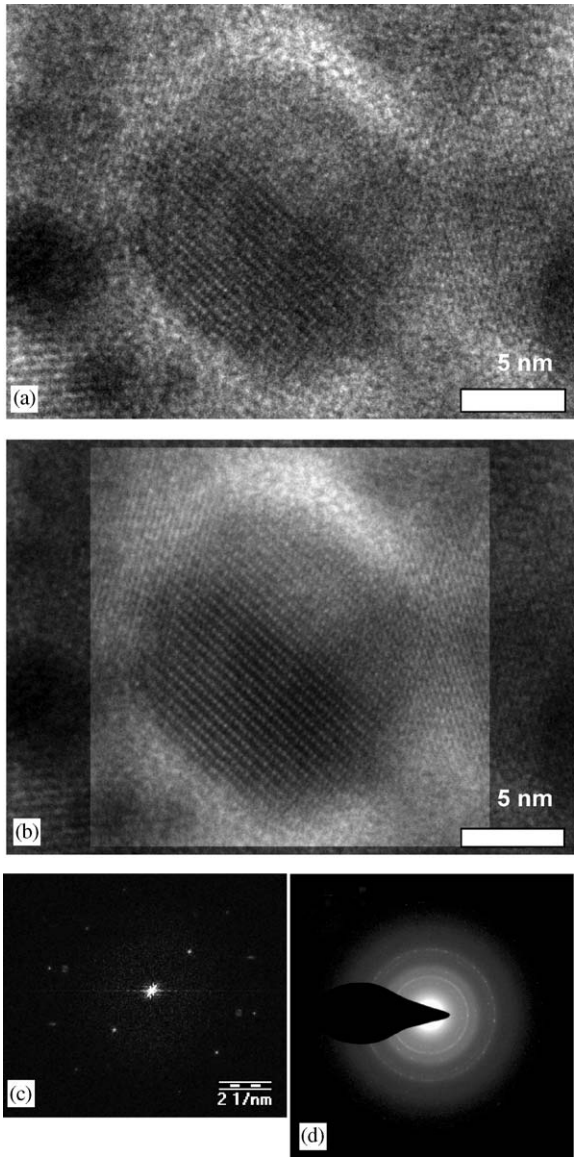

Fig. 8. Bright-field TEM image of a FeCoPt particle (a) with its FFT filtered image (c) and the corresponding fast Fourier transformation (FFT) pattern and filtered FFT-image. The diffraction image and the FFT pattern (c) and (d) prove the crystallinity of the FeCoPt particles.

4. Results and discussion

Currently, FePt nanoparticles have been prepared with different shapes as can be seen in Fig. 2. In the area where only spheres are assembled (Fig. 2a) the mean particle diameter of the spheres is $\langle D\rangle = 4.23 \pm 0.12$ nm and the averaged distance from particle surface to particle surface is $\langle d\rangle = 2.15 \pm 0.99$ nm. Measuring the diameters of the nanospheres and nanocubes produced inherent detectable in Fig. 2b, results in a size distribution with a mean diameter of $\langle D\rangle = 4.47 \pm 1.73$ nm for the spheres and $\langle D_{cubes}\rangle = 18.5 \pm 1.75$ nm for the cubes. The particle center to center distance has a value of $\langle C\rangle = 5.78 \pm 0.11$ nm. Energy dispersive X-ray analyses (Fig. 3b) reveals that the composition of these FePt nanocube is about

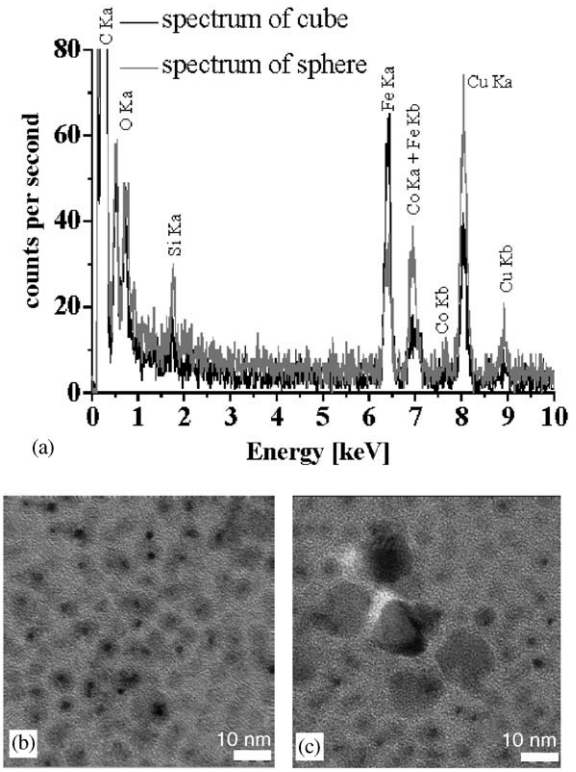

Fig. 9. The compositions of the different shaped particles ((c) cube $Fe_{75}Co_{25}$, (b) spheres $Fe_{50}Co_{50}$) has been measured by EDX (a) at HRTEM in Nanoprobe mode (spotsize $\approx$10 nm). From this a concentration versus particle size dependency is obvious.

$Fe_{50}Pt_{50}$ although the charged ratio of Fe:Pt had been 2:1.

In Fig. 4a are 5 nm sized nanospheres and a bigger FePt nanocube with a measured square length of 18.83 nm and a lattice spacing of $\langle d_{hkl}\rangle = 0.277 \pm 0.027$ nm observable. This d_{hkl} value is similar to the measured lattice-plane spacing $d_1 = 0.2750$ nm belonging to the FePt nanosphere. Comparing the measured lattice plane constants with the ones given in literature in this case a $FePt_3$ FCC (1 0 0) orientation ($d_{hkl} = 0.2736$ nm $\pm$ 1% [14]) is identified, because a deviation from the literature value of 1% is reached. The FePt nanoparticles have not been annealed thus to verify the disordered cubic phase is found. This cubic phase is also found by XRD measurement where the different peaks are all probably belonging to either FePt or $FePt_3$ FCC phase as it can be seen in detail below. The estimated theoretical particle sizes match pretty good with the diameters determined by TEM measurements. Interesting in the image Figs. 4b and c is that there is a rotation moiré observable at the nanosphere. It originates from the superposition of two different lattice-plane spacings which are rotated by a small angle to each other with the foil normal as axis [11]. Besides the lattice-plane spacing $d_1 = 0.2750$ nm the moiré-lattice constant $d_M = 1.9$ nm and the rotation angle $\alpha = 8.79^\circ$ are measured, too. The moiré-fringe spacing of d_M depends on the lattice-plane spacings d_1 and d_2 as given in Eq. (1) so that the lattice-plane spacings d_2 could easily be calculated to 0.2090 nm. The calculated lattice constant could be possibly Fe FCC (1 1 0) with $d_{hkl} = 0.20182$ nm $\pm$ 3.5% [14] or $FePt_3$ FCC (2 0 0) with $d_{hkl} = 0.1934$ nm $\pm$ 7.5% [14] or FePt FCC (1 1 1) with $d_{hkl} = 0.2202$ nm $\pm$ 5.4% [14] due to the accuracy of the calculation. Latter phase is most probable, because FePt FCC peaks are also found in the XRD diffractogram (Fig. 3a) and the EDX measurement (Fig. 3b) reveals a composition

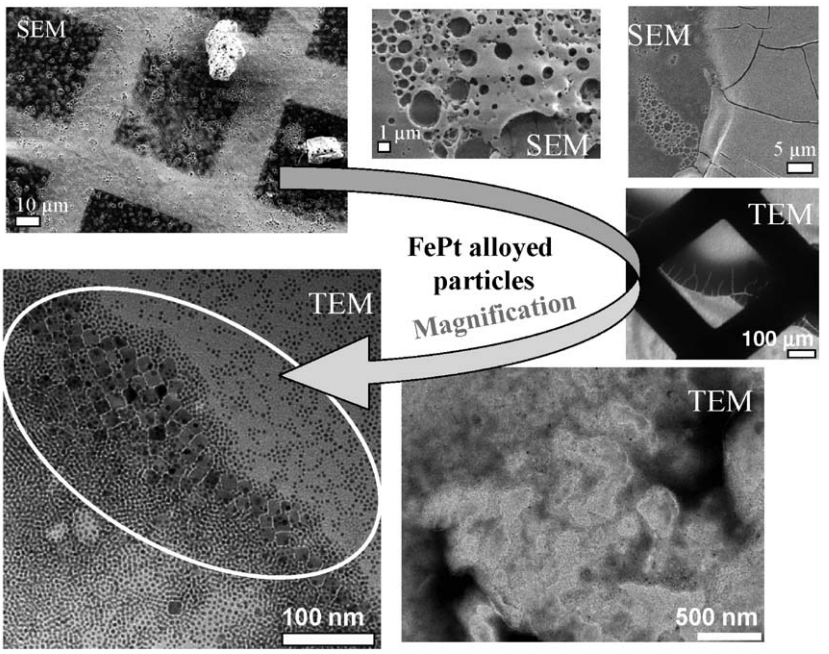

Fig. 10. Series of scanning electron microscopy (SEM) and transmission electron microscopy (TEM) images taken from the identical $Fe_{50}Pt_{50}$ particles deposited on a TEM copper grid. Whereas the nanoparticles in this particular case could not be resolved by SEM (high tension 5 kV), because of the crusty material, the same particles could be imaged nicely by TEM (high tension 200 kV) because the material could be transmitted.

of the particles of $Fe_{50}Pt_{50}$.

$$d_M = \frac{d_1 d_2}{(d_1^2 + d_2^2 - 2d_1 d_2 \cos\alpha)^{1/2}}. \quad (1)$$

The results of FeCoPt nanoparticles produced in different ways are compared to each other under the aspects of growth mechanism, size distribution and crystal structure. In Fig. 5 the bright-field images of $Fe_4Co_2Pt_1$ nanoparticles are given with their corresponding size distributions. For Fig. 5b EDX by HRTEM analysis reveals a composition of $Fe_{2.8}Co_{1.0}Pt_{4.4}\pm5\%$ for the particles prepared by PM2. From the LogNormal size distribution a mean particle diameter $\langle D\rangle = 0.95 \pm 0.59$ nm has been determined. The mean particle diameter of $Fe_{1.8}Co_{1.0}Pt_{5.5}\pm5\%$ particles prepared by PM3 is $\langle D\rangle = 4.63 \pm 0.34$ nm (Fig. 5a). The same sample of $Fe_{1.8}Co_{1.0}Pt_{5.5}\pm5\%$ (PM3) deposited on a silicon oxide substrate show XRD-peaks (marked in Fig. 6a) belonging to either $CoPt_3$ FCC phase or FePt FCC or $FePt_3$ FCC. The lattice parameters $a = 0.3833(1)$ nm and $c = 0.3718(1)$ nm of the low temperature AuCu like $CoFePt_2$ is given in Ref. [15]. And from this lattice parameter it has been possible by the formula of Bragg to determine the characteristic peak positions of this $CoFePt_2$ phase. With this information the XRD data could be analyzed as can be seen in Fig. 6b so that there is obviously a $CoPt_3$ FCC phase or a $CoFePt_2$ phase present. At last the XRD analyses in Fig. 7a clearly show that these FeCoPt nanoparticles prepared by PM4 are crystallized into the $CoFePt_2$ phase with the peak positions of circa 20° belonging to the (1 1 1) orientation and circa 35° to (2 0 2) orientation. The mean particle diameter quantified by the TEM bright-field image given in Fig. 7b is $\langle D\rangle = 5.66 \pm 0.76$ nm. The given lattice plane spacings of the nanoparticle in Figs. 8a and b have been determined by measuring them ($d_1 = 0.2513$ nm, $d_2 = 0.2921$ nm, $d_3 = 0.2525$ nm, $d_4 = 0.2510$ nm, $d_5 = 0.2550$ nm) or by analyzing the moiré-fringe (lattice-plane spacing $d_6 = 0.2915$ nm, $d_7 = 0.2859$ nm, the moiré-lattice constant $d_M = 0.5096$ nm and the rotation angle $\alpha = 90°$) in the same way as above. Due to large values of the lattice plane spacings and the accuracy of the calculation the particle possibly contains $CoFePt_2$ or any Fe oxide (FeO or Fe_2O_4). The diffraction image and the FFT pattern (Figs. 8c and d) prove the crystallinity of the FeCoPt particles. The compositions of the different

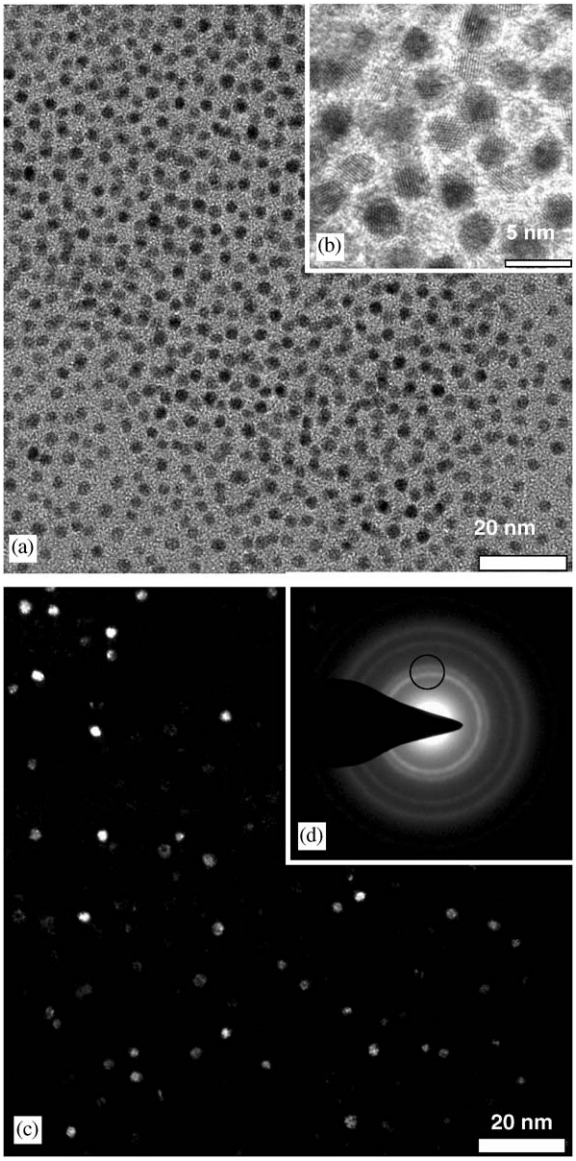

Fig. 11. (High-resolution) bright-field (BF) (a, b) and dark-field (DF) (c) TEM images of FePt nanoparticles. The circle in the diffraction pattern (d) should demonstrate the position of the aperture which has been set to produce this dark-field image. The structures found in the DF image are all belonging to the diffraction rings selected before.

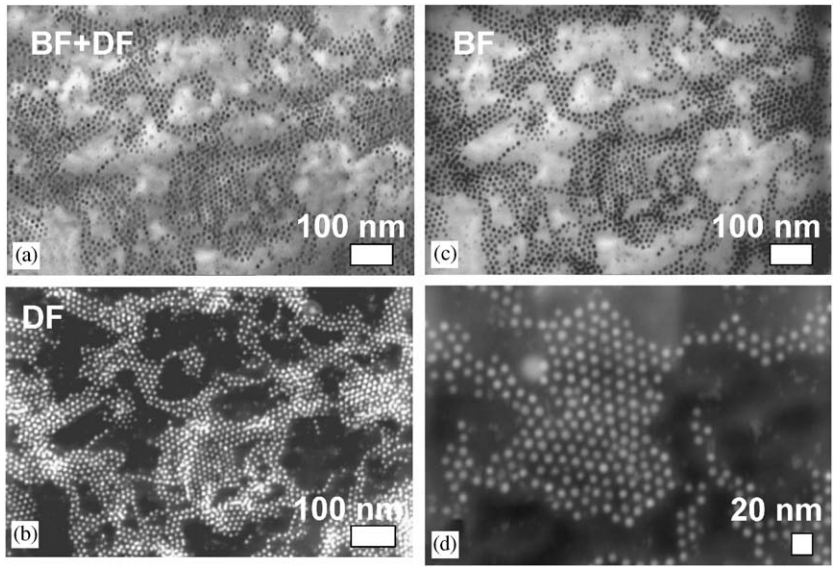

Fig. 12. Prospect of cobalt nanoparticles made in STEM mode with a working voltage of 27 keV and a small working distance of 2 mm in different image modes and resolutions: bright-field image (a), dark-field image (b) and the combination of both (c). A high-resolution image of the monodisperse spheres is given in (d).

shaped particles (cube $Fe_{75}Co_{25}$ (Fig. 9c), spheres $Fe_{50}Co_{50}$ (Fig. 9b)) has been measured by HRTEM in Nanoprobe mode (spotsize $\approx$10 nm) (Fig. 9). The platinum content could not be determined because in this exemplary case the concentration of the platinum cluster prepared separately had been too low. From all this a concentration versus particle size dependency is obvious. The series of scanning electron microscopy (SEM) and transmission electron microscopy (TEM) images taken from the identical $Fe_{50}Pt_{50}$ particles deposited on a TEM copper grid shown in Fig. 10 demonstrate the advantages of using higher energies for getting insights into the samples if someone compares the different microscopic methods SEM to STEM to TEM with increasing acceleration voltages and magnifications. Whereas the nanoparticles in this particular case could not be resolved by SEM (high tension 5 kV), because of the crusty material due to byproducts which arising from the reduction of the platinum acetylacetonate the same particles could be imaged nicely by TEM (high tension 200 kV) where the material could be transmitted. In Fig. 11 (high-resolution) bright-field (BF) (Figs. 11a and b) and dark-field (DF) (Fig. 11c) TEM images of FePt nanoparticles are presented. The structures found in the DF image are all belonging to the diffraction rings selected before (Fig. 11d). In the same manner as bright- and dark-field images could be made by TEM it is possible to see the nanoparticles with different contrasts by STEM. Prospect of cobalt nanoparticles made in STEM mode with a working voltage of 27 keV and a small working distance of 2 mm in different image modes and resolutions is given in Fig. 12. STEM mode allows a comfortable imaging of approximately a dozen of electron transparent specimens in SEM microscopes at the same time with a better resolution through the reduction of the information volume.

Over all, because of the less-time consuming work the scanning transmission electron microscopy should be favored for investigating nanoparticles. Nevertheless, transmission electron microscopy stays to be necessary aiming for high-resolution to reveal the microstructure.

Additionally, electron energy-loss spectroscopy (EELS) was employed to determine the oxide content of the particle surface layer. Fig. 13 shows the bright-field image and the corresponding EELS-spectra of a FePt nanoparticle sample with its iron to oxygen ratio. The oxygen K-edge at $\sim$532 eV and Fe-$L_{3,2}$ edges observed at 708 and

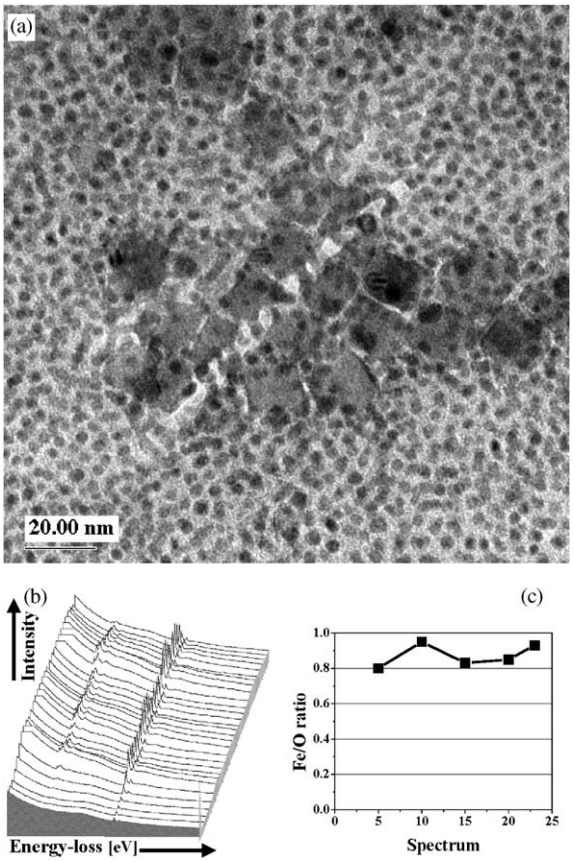

Fig. 13. Bright-field image (a) and the corresponding EELS-spectra (b) of a FePt nanoparticle sample with its iron to oxygen ratio (c).

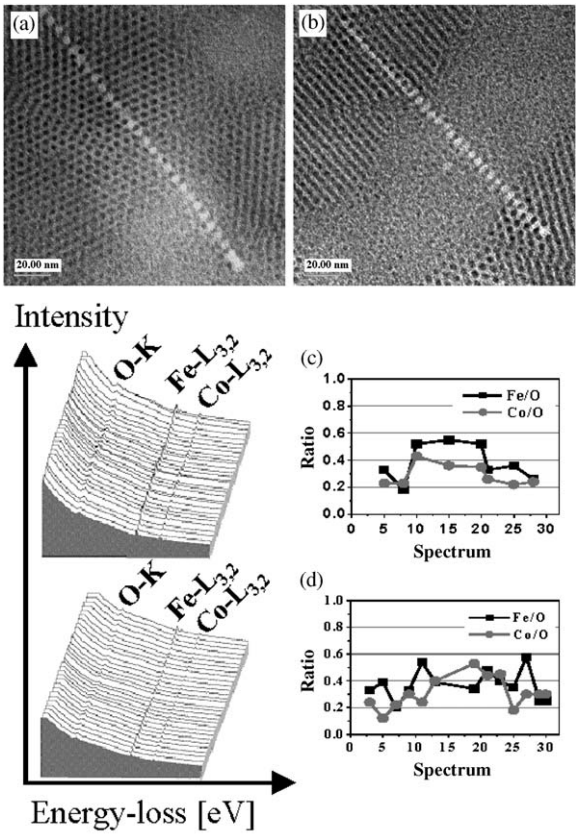

Fig. 14. Bright-field images (a,b) and the corresponding EELS-spectra of a FeCo nanoparticle sample with their iron to oxygen and cobalt to oxygen ratios (c,d).

721 eV indicate that the particles consist of Fe oxide. Platinum could not be identified because the Pt–N_5 edge is positioned by ~315 eV [16] which is lower than the nominal energy used for the measurement. Despite this, the question if the Pt–N_5 edge is resolvable, is considered by Sobal [17]. It is reported that it could not be analyzed, because of the poor intensity and the superposition with the very intensive CIS edge of carbon. The concentration graph (Fig. 13c) does not show large variations of the Fe/O ratio across the zone analyzed. This is due to the fact that the particles are more or less all of the same size.

Two different EELS measurements of FeCo particles are shown in Fig. 14 in which the Fe-$L_{3,2}$ edges could be observed at 708 and 721 eV and the Co-$L_{3,2}$ edges observed at 778 and 794 eV which indicates the alloying, too. Contrary to the FePt particles especially from the concentration ratio of Fe/O and Co/O across spectra, it can be followed that the degree of oxidation is less in the zones of smaller particles (zones in the figures above where no clear particles are seen).

5. Conclusion

The different microscopic techniques have been compared and discussed under the main aspects of contrast and resolution to aim the individual

investigation of magnetic carriers with respect to the microstructure, particle size distribution and composition. The combination of all analytical electron microscopy techniques reveal closer insights into the chemical and physical properties of alloyed magnetic nanoparticles as it is presented here. Finally, the analytical electron microscopy results show that the magnetic carrier are binary or ternary $(Fe_{1-x}Co_x)_{1-y}Pt_y$ alloyed nanoparticles with spherical and cubic shapes and a small size distribution that is important for any potential application.

References

[1] A. Hütten, D. Sudfeld, I. Ennen, et al., J. Biotechnol. 112 (2004) 47.
[2] A. Hütten, D. Sudfeld, I. Ennen, et al., J. Magn. Magn. Mater. (2005) this issue, doi:10.1016/j.jmmm.2005.01.048.
[3] V.F. Puntes, K.M. Krishnan, A.P. Alivisatos, Science 291 (2001) 2115.
[4] C.B. Murray, S. Sun, W. Gaschler, et al., IBM J. Res. Dev. 45 (2001) 47.
[5] D.P. Dinega, M.G. Bawendi, Angew. Chem. 111 (1999) 1906.
[6] S. Sun, C.B. Murray, D. Weller, et al., Science 287 (2000) 1989.
[7] S. Sun, C.B. Murray, H. Doyle, Mater. Res. Soc. Symp. Proc. 577 (1999) 385.
[8] M. Shinkai, J. Biosci. Bioeng. 94 (2002) 606.
[9] M. Chen, D. Nikles, Nano Lett. 2 (2002) 211.
[10] D. Sudfeld, I. Ennen, W. Hachmann, et al., Microscopy Microanal. 9 S03 (2003) 196.
[11] L. Reimer, Transmission Electron Microscopy, fourth ed., Springer, Berlin, 1997.
[12] B. Fultz, J.M. Howe, Transmission Electron Microscopy and Diffractometry of Materials, second ed., Springer, Berlin, 2002.
[13] Scherrer, Goettinger Nach. 2 (1918) 98.
[14] Reference database, International Centre for Diffraction Data, 1999.
[15] P. Villars, L.D. Calvert, Pearson's Handbook of Crystallographic Data for Intermetallic Phase, 1996.
[16] Lawrence Berkeley National Laboratory, X-ray Data Booklet, second ed., 2001.
[17] N. Sobal, Ph.D. Thesis, Berlin, 2003.